25 January 2023

Intrinsic Millisecond Kinetics of Polyethylene Pyrolysis via Pulse-Heated Analysis of Solid Reactions

Isaac Mastalski[1], Nathan Sidhu[1], Ali Zolghadr, Saurabh Maduskar[2], Bryan Patel[2], Sundararajan Uppili[2], Tony Go[2], Ziwei Wang[1], Matthew Neurock[1], Paul Dauenhauer[1]

1. University of Minnesota

2. ExxonMobil Chemical Company

Abstract

Continued demand for polyolefins can be met by recycling plastic materials back to their constituent monomers, ethylene and propylene, via thermal cracking in a pyrolysis reactor. During pyrolysis, saturated polyolefin chains break carbon-carbon and carbon-hydrogen bonds, yielding a distribution of alkanes, alkenes, aromatic chemicals, light gases, and solid char residue at temperatures varying from 400-800 °C. To design a pyrolysis reactor that optimizes the chemistry for maximum yield of light olefins, a detailed description of the chemical mechanisms and associated kinetics is required. To that end, the reaction kinetics of isothermal films of low-density polyethylene (LDPE) have been measured by the method of 'Pulse-Heated Analysis of Solid Reactions,' or PHASR, which allows for quantification of intrinsic kinetics via isothermal reaction-controlled experimental conditions. The evolution of LDPE films from 20 milliseconds to 2.0 seconds for five temperatures (550, 575, 600, 625, and 650 °C) was characterized by measurement of the yield of chromatography-detectable compounds (<C20) in addition to the total yield of volatile products. The kinetics of volatile product evolution was interpreted via a lumped kinetic model with activation energy 225 ± 16 kJ/mol, compared with existing kinetic models of polyethylene pyrolysis, and validated from first principles.

Keywords

flash pyrolysis, kinetics, polyethylene, pyrolysis, recycling

Intrinsic Millisecond Kinetics of Polyethylene Pyrolysis via Pulse-Heated Analysis of Solid Reactions

Isaac Mastalski[1,†], Nathan Sidhu[1,†], Ali Zolghadr[1], Saurabh Maduskar[2], Bryan Patel[2], Sundararajan Uppili[2], Tony Go[2], Ziwei Wang[1], Matthew Neurock[1], Paul J. Dauenhauer[1,*]

[1] University of Minnesota, Department of Chemical Engineering & Materials Science, 421 Washington Avenue SE, Minneapolis, MN, USA 55455

[2] ExxonMobil Technology and Engineering Company, 5200 Bayway Drive, Baytown, TX, USA 77520

[†] Authors contributed equally

[*] Corresponding author: hauer@umn.edu

Abstract. Continued demand for polyolefins can be met by recycling plastic materials back to their constituent monomers, ethylene and propylene, via thermal cracking in a pyrolysis reactor. During pyrolysis, saturated polyolefin chains break carbon-carbon and carbon-hydrogen bonds, yielding a distribution of alkanes, alkenes, aromatic chemicals, light gases, and solid char residue at temperatures varying from 400-800 °C. To design a pyrolysis reactor that optimizes the chemistry for maximum yield of light olefins, a detailed description of the chemical mechanisms and associated kinetics is required. To that end, the reaction kinetics of isothermal films of low-density polyethylene (LDPE) have been measured by the method of 'Pulse-Heated Analysis of Solid Reactions,' or PHASR, which allows for quantification of intrinsic kinetics via isothermal reaction-controlled experimental conditions. The evolution of LDPE films from 20 milliseconds to 2.0 seconds for five temperatures (550, 575, 600, 625, and 650 °C) was characterized by measurement of the yield of chromatography-detectable compounds (<C20) in addition to the total yield of volatile products. The kinetics of volatile product evolution was interpreted via a lumped kinetic model with activation energy 225 ± 16 kJ mol^{-1}, compared with existing kinetic models of polyethylene pyrolysis, and validated from first principles.

1.0 Introduction. Large-scale production of plastics developed in the 1950s, and their necessity for modern life is visible today, with plastics providing functionality in products critical to society. An estimated 8.3 billion tons of raw plastics had been made through 2017, with over 25 billion tons projected to be generated by 2050.[1] In the linear plastic economy model that currently defines polymer production, utility, and material end of life, nearly all plastics end up being landfilled, with only about 10% being recycled.[1] The current polymer system provides an opportunity for developing a new, circular plastic economy, whereby used plastics can be continuously remade into new raw materials in an efficient and cost-effective manner.[2–6]

Of particular importance for a circular plastic economy is polyethylene (PE), which accounts for ~29% of all plastics that are made and ~51% of all plastic packaging.[1,7] Plastic packaging, which is frequently intended for single-use applications, comprises ~38% of all plastic production, making it a significant opportunity for plastic recycling.[1,7] Because of the abundance of polyethylene, and in particular the low-density variant (LDPE), which makes up ~16% of all plastic globally and ~30% of all plastic packaging, LDPE is the primary focus of this work, though the methods detailed herein can be applied to other plastic materials.[7,8]

LDPE is not recycled at a rate commensurate with its production level due to many challenges in the recycling process. Mechanical recycling is the most common recycling method, with plastics separated by type, melted down, and extruded into pellets for sale to manufacturers. But with each cycle through the mechanical recycling process, the structural integrity of the plastic decreases due to polymer chains being inadvertently broken down.[9,10] Therefore, virgin LDPE must be added to recycled LDPE to improve performance, and LDPE

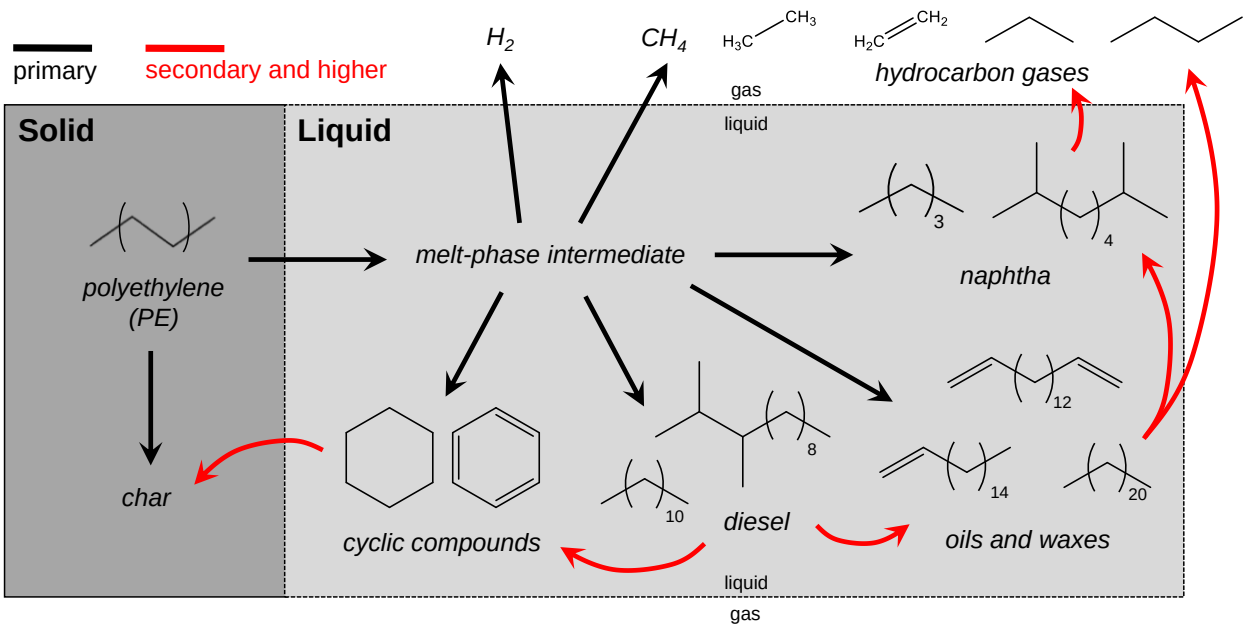

Figure 1. Thermal decomposition of polyethylene to liquids, vapors, and char by primary (black arrows) and secondary (red arrows) reaction pathways.

can only pass through this cycle a handful of times before its quality is too low for further value-added recycling; alternatively, recycled plastics that are not mixed with virgin plastic must be 'downcycled' and used in lower-value applications.[9] Additionally, additives and post-processing impurities in plastic streams present further challenges for mechanical recycling, and the overall economic viability of mechanical recycling often suffers due to the need for costly pre-sorting stages.[11,12]

Alternatively, chemical recycling methods decompose polymers back to their constituent monomers, which can be reconstituted into new polymers without a decrease in polymer performance. Through pyrolysis, one such chemical recycling method, waste plastics are thermally degraded in an inert atmosphere; the lack of oxygen prohibits the formation of undesirable products like CO, CO_2, and oxygen-functionalized hydrocarbon species.[13] However, the radical reactions that occur during pyrolysis generate a highly complex mixture of products via a poorly understood network of reactions. **Figure 1** illustrates just a few of the numerous compounds that have been reported in the literature. In general, LDPE first passes through a depolymerized melt-phase intermediate rich in radical species.[14,15] These radicals react to form primary products (**Figure 1**, black pathways), after which these primary products can also form secondary and higher order products (**Figure 1**, red pathways) through further reaction and interconversion.[16–22]

Despite consensus on the radical nature of polyethylene pyrolysis chemistry, the underlying chemical pathways and the extent to which different reactions (e.g., H-transfer, β-scission) occur remain unknown.[21,23–26] Significant variation exists in the literature regarding the kinetic parameters that define the rate of formation of polyolefin chemical products. As evidenced by **Figure 2**, the apparent activation energy and pre-exponential factor for polyethylene pyrolysis from 47 different publications and 191 individual data points vary predominantly in the range of ~160 to ~310 kJ mol^{-1} and 10^9 to 10^{21} s^{-1}, respectively; more information for this figure is provided in the Supporting Information. The discrepancies in reported kinetics likely arise from a combination of sources.[18,20,23,27–31] Polyethylene samples with large length scales (i.e., thick films, pellets, packed powders) introduce heat and mass transfer limitations that exhibit a distribution of reaction kinetics throughout a pyrolyzing polyolefin particle. Reactor designs with long gas-phase residence times can permit secondary and higher order reactions, and the distribution of temperature within different reactors can limit the transfer of

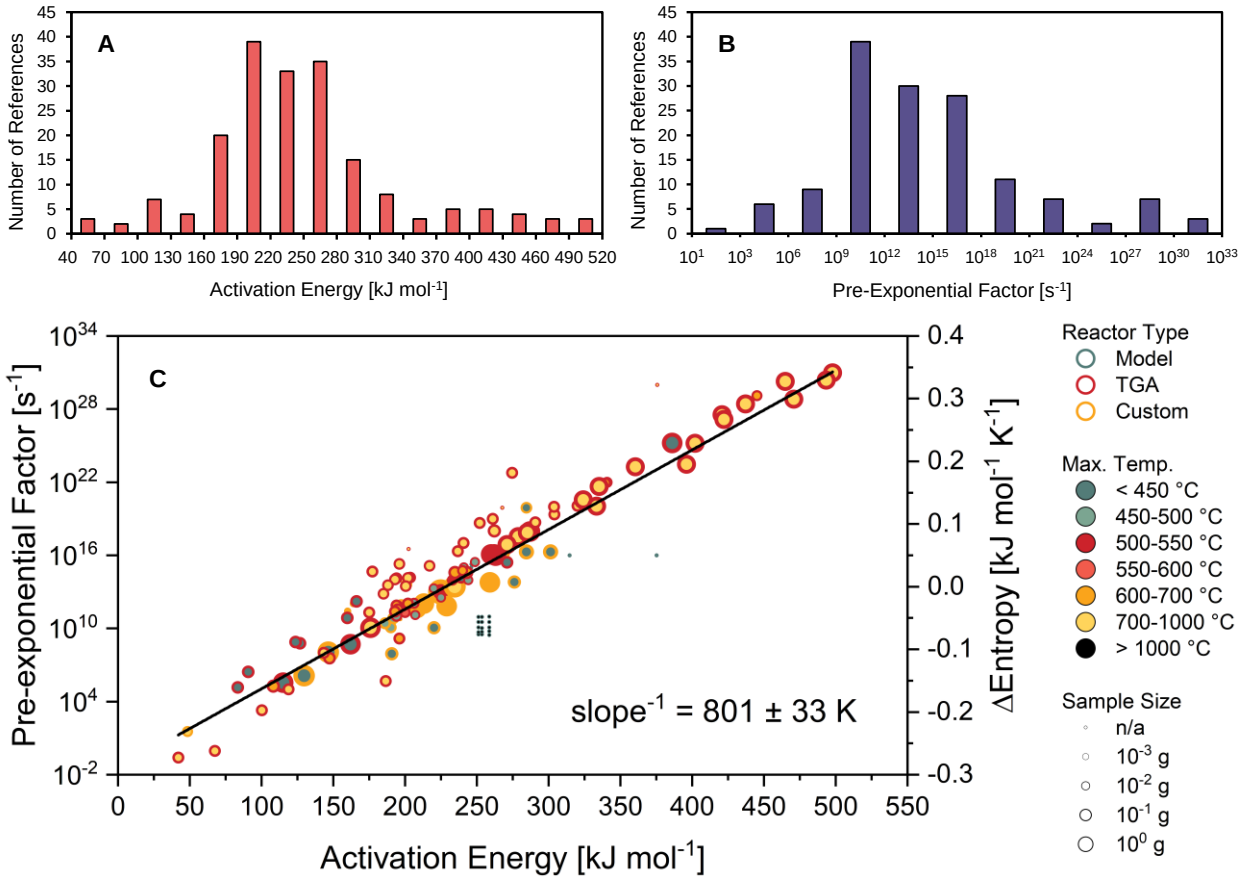

Figure 2. Literature-reported lumped kinetics of polyethylene pyrolysis. (A) Apparent activation energy. (B) Apparent pre-exponential factor. (C) Compensation of activation energy and pre-exponential factor with secondary axis of apparent entropy of activation.

some chemical products to the reactor exit. Additionally, some reaction methods, such as thermogravimetric analysis (TGA), use a thermal ramping (e.g., 10 K min^{-1}) whereby the polyethylene sample proceeds through reactions at a range of chemistries before achieving the high temperatures of interest (>500 °C). Due to these experimental limitations, the literature presently reports the apparent kinetics of polyethylene pyrolysis, as opposed to the intrinsic kinetics, which are necessary for elucidating reaction pathways and developing scalable, consistent reactors for recycling applications.

To measure the intrinsic kinetics of polyethylene pyrolysis, we used an experimental system called the Pulse-Heated Analysis of Solid Reactions (PHASR) reactor, which eliminates transport limitations during polyolefin pyrolysis through the use of a thin film sample and rapid sample heating and cooling. With integrated resistive heating and conductive cooling of the reacting sample film, PHASR applies short (20 ms to 2.0 s) thermal pulses of defined temperature to samples, after which the reacting melt and resultant vapor products are thermally quenched and analyzed. PHASR was originally developed for cellulose pyrolysis[32] and has since been redesigned for application to polyolefin pyrolysis with higher temperatures (>700 °C) and heavier hydrocarbon products.[8] In this work, application of PHASR to LDPE pyrolysis was evaluated to ensure isothermal, reaction-controlled operation. Thereafter, the rate of formation of products was measured for reaction durations of 20 ms to 2.0 seconds at temperatures from 550 to 650 °C. The kinetic results were then compared with observations reported in the literature.

2.0 Methods. A complete description of the PHASR system is presented elsewhere,[8] but the method of PHASR is summarized as follows. A thin film of LDPE (3.0 mm diameter, 15 μm

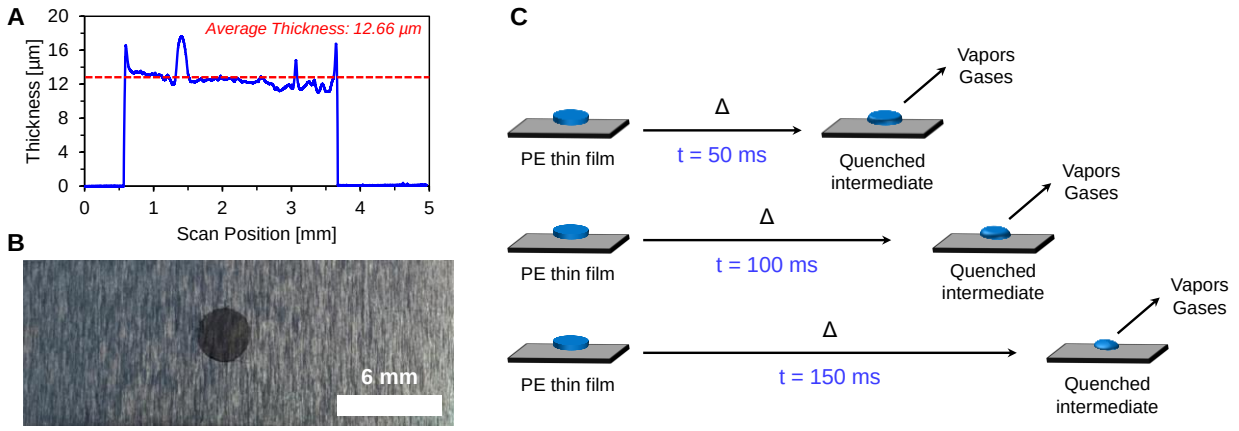

Figure 3. Low-density polyethylene thin film samples. (A) Thin-film profilometry of a low-density polyethylene sample reveals an average thickness of ~13 µm across the full 3.0 mm sample diameter. (B) Photograph of low-density polyethylene film sample (~15 µm thick, 3.0 mm diameter) deposited on passivated steel plate in preparation for reaction in PHASR. (C) Vapor and gas product generation from polyethylene films during variable reaction durations of 50, 100, and 150 ms.

thickness) was deposited on a passivated carbon steel plate. Copper electrodes contacted the plate, delivering a pulse of electricity and resistively heating it to a desired reaction temperature (up to 700 °C, in <20 ms) for a desired length of time (from 20 ms up to 2.0 s) with a temporal resolution of 10 ms. An optical pyrometer directly above the sample monitored its temperature for control through a 1000 Hz PID feedback loop. Under the steel sample plate, a thin piece of aluminum nitride ceramic electrically insulated the sample from a gold-plated heat exchanger, through which a synthetic coolant (Sylltherm 800, Dow) continuously flowed to rapidly cool the sample down to room temperature and quench the reaction (<180 ms). The body of the reactor was held at 300 °C to reduce product condensation, and a constant stream of He (~360 mL min^{-1}) flowed across the sample to sweep volatile product species into an attached gas chromatograph/Polyarc/flame ionization detector (GC/PA/FID) for analysis.[8]

Samples in this study were prepared from LDPE pellets (~2 mm diameter; ~100,000 g mol^{-1} M_w determined by light scattering; 0.8 weight% ash determined by ICP) provided by the ExxonMobil Technology and Engineering Company. These pellets were flattened in a Mini-Film Maker (Specac, Ltd.; 115 °C, 0.5 tons force, 30 s) into discs with a diameter of about 1.5 cm and a thickness of about 15 µm, as verified by surface profilometry results shown in **Figure 3a**. A circular, 3.0 mm diameter punch was then used to cut the final 3.0 mm diameter samples from the larger discs for use in PHASR. A modified method was used to prepare even thinner samples for preliminary testing, whereby the 15 µm thick, 3.0 mm diameter discs were pressed again in the Mini-Film Maker (100 °C, 1 ton force, 30 s). The resulting film was ~8 µm thick with a diameter of ~4 mm; surface profilometry results for this are shown in the Supporting Information. Finalized samples were then weighed on a microgram-resolution balance (Mettler Toledo XPR2U) to precisely determine initial weight; all samples were within the range of 80 ± 10 µg. Meanwhile, 1010 carbon steel plates (1" x 3/8" x 0.007") were cleaned with isopropyl alcohol and passivated with a butane torch. The finalized LDPE samples were then deposited on the steel plates at 120 °C to ensure good thermal contact; a photograph of a finished plate with sample is shown in **Figure 3b**.

After the LDPE samples were deposited on the passivated steel plates, the plates were loaded into the PHASR reactor, and reactions were conducted in the manner described above, consistent with previous work.[8] During reaction pulses, the body of the PHASR reactor was held constant at 300 °C via a series of cartridge heaters located throughout the reactor body, and the temperature of the LDPE sample was recorded by an optical pyrometer; **Figure 3c** illustrates the reaction progression during the experiment. Upon completion of each experimental trial, the steel plates were removed from PHASR, trimmed to a smaller size (to enhance weighing accuracy) and weighed on the XPR2U balance. The residue left behind after reaction was

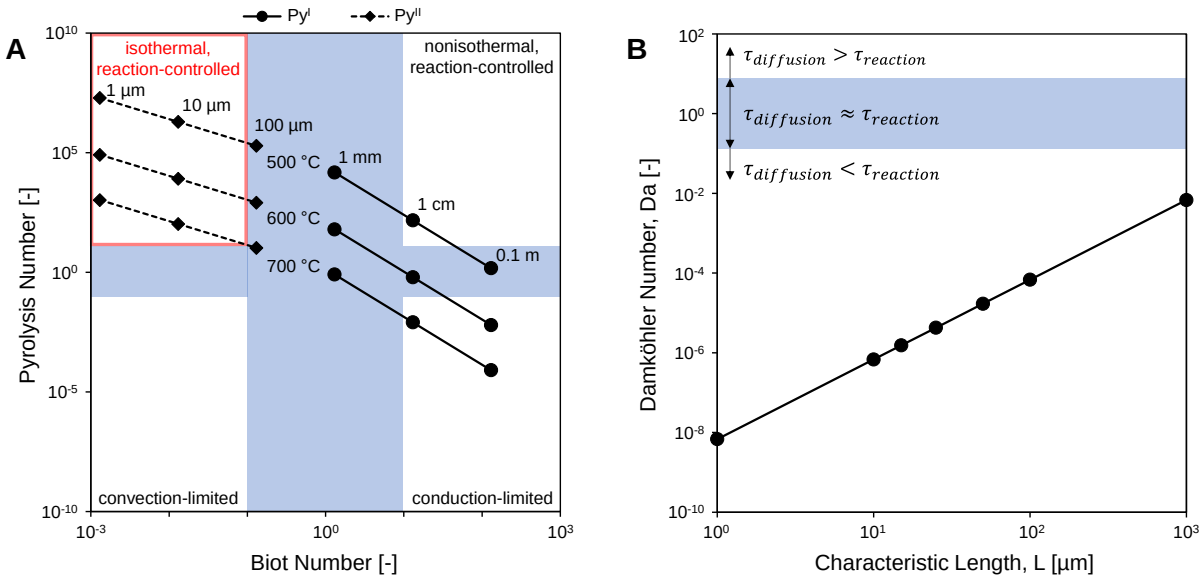

Figure 4. Dimensional analysis of reacting polyethylene films. (A) Heat transport map depicting the pyrolysis numbers (PyI and PyII) versus the Biot number. (B) Mass transport map depicting the Damköhler number versus the characteristic polyethylene length scale (i.e., film thickness). See Supporting Information for assumptions on both figures.

then removed by soaking the steel plates in 1,2,4-trichlorobenzene (TCB, 99%, Alfa Aesar) at 150 °C for 15 min. After the plates dried in ambient air, they were weighed again; the difference between post-reaction weight and post-cleaning weight was the weight of residue left behind, and the difference between initial sample weight and weight of residue left behind was the weight of LDPE that was reacted and volatilized. Due to the significantly larger mass of steel plate with residue (order 100,000 µg), all post-reaction measurements with the XPR2U balance were conducted in duplicate and averaged to enhance precision, with a difference between duplicates of <0.5 µg.

For the present work, at least three individual samples for each data point were reacted across a range of reaction durations (i.e., 20 ms to 2.0 s, with an emphasis on shorter timescales to improve resolution of initial reaction kinetics) and reaction temperatures (550 to 650 °C in 25 °C increments). Products reported herein are categorized as "GC-detected" (i.e., light species consisting of all hydrocarbon products up to C20), "microbalance-detected" (i.e., heavier species that volatilized off the sample plate but condensed within the GC/PA/FID), and "residue" (i.e., char, other non-volatilized species, and any unreacted LDPE left behind on the sample plate and removed with TCB during the post-reaction cleaning process), as described in previous work.[8]

3.0 Results and Discussion.

3.1 Validation of PHASR Application to LDPE Pyrolysis. Isothermal, reaction-controlled conditions are required for obtaining intrinsic reaction kinetics. To ensure that these conditions were met within the PHASR reactor, both theoretical and experimental analyses of the transport properties of the LDPE samples were performed. **Figure 4a** plots the pyrolysis numbers against the Biot number, providing a dimensional analysis for heat transport within the LDPE system. The two pyrolysis numbers compare the timescales of reaction to conduction and convection (Py^{I} and Py^{II}, respectively), and the Biot number (Bi) compares the timescale of conduction to convection. Further detail, including the definitions of the dimensionless quantities and selected parameters, is provided for these calculations in the Supporting Information. The top left quadrant of **Figure 4a**, outlined in red, depicts the isothermal, reaction-controlled regime, in which conductive heat transport is faster than convective heat transport, and convective heat transport is much faster than reaction. This order of magnitude

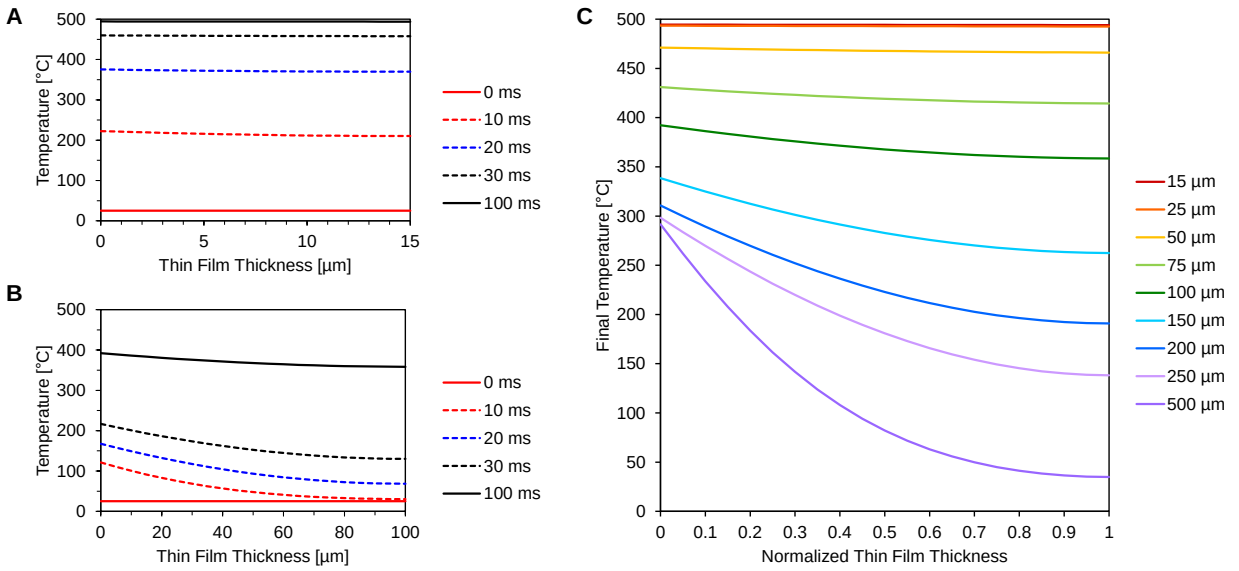

Figure 5. One-dimensional reaction-conduction transient temperature profiles from simulation. (A) 15 µm thick sample with a target temperature of 500 °C. (B) 100 µm thick sample with a target temperature of 500 °C. (C) Final temperatures for samples of different thicknesses after 100 ms and a target temperature of 500 °C. See Supporting Information for complete simulation details.

estimate indicates that LDPE samples up to order 100 µm in thickness can be pyrolyzed at temperatures up to 700 °C to obtain intrinsic kinetics. A similar approach can be taken to dimensionally analyze mass transport within an LDPE film sample; **Figure 4b** plots the Damköhler number against the characteristic length scale of the sample (i.e., sample thickness). Calculations for the Damköhler number are provided in the Supporting Information. The order of magnitude estimate of **Figure 4b** indicates that a sample thickness of 15 µm will permit diffusion of alkanes orders of magnitude faster than the reaction timescale. Both of these analyses rely on estimates of the parameters of reaction, heat, and mass transfer, provided elsewhere in the literature and identified in the Supporting Information.

Further analysis was conducted using a 1-D heat transfer simulation in MATLAB. The simulation of a film of low-density polyethylene accounts for the reaction kinetics throughout the film, heat conduction through the film, and heat transfer at the film/reactor and film/vapor interfaces. Complete details for the simulation can be found in the Supporting Information, including the selected simulation parameters. **Figure 5a** plots the temperature profile through the film after varying reaction pulse durations for 15 µm thick LDPE samples. After just 20 ms, samples are within about 100 °C of the 500 °C reaction temperature of the sample plate, and they approximately reach that set point within 30 ms. The importance of sample thickness is further substantiated by **Figure 5b**, which plots the same data as **Figure 5a**, but for a sample that is 100 µm thick instead of 15 µm. It is clear that even after 100 ms, this thicker film

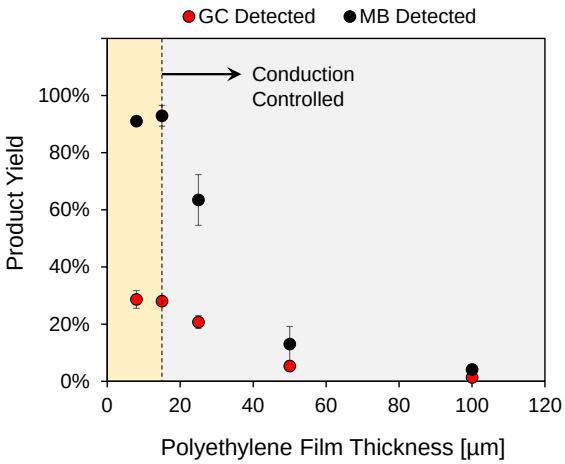

Figure 6. Experimental yield of volatile products detected by both a gas chromatograph (GC, red) and microgram-resolution balance (MB, black) as a function of polyethylene film thickness at a reaction temperature of 650 °C and a duration of 100 ms. Experiments are reaction-controlled for films thinner than 15 µm (yellow region) and conduction-controlled for films thicker than 15 µm (gray region).

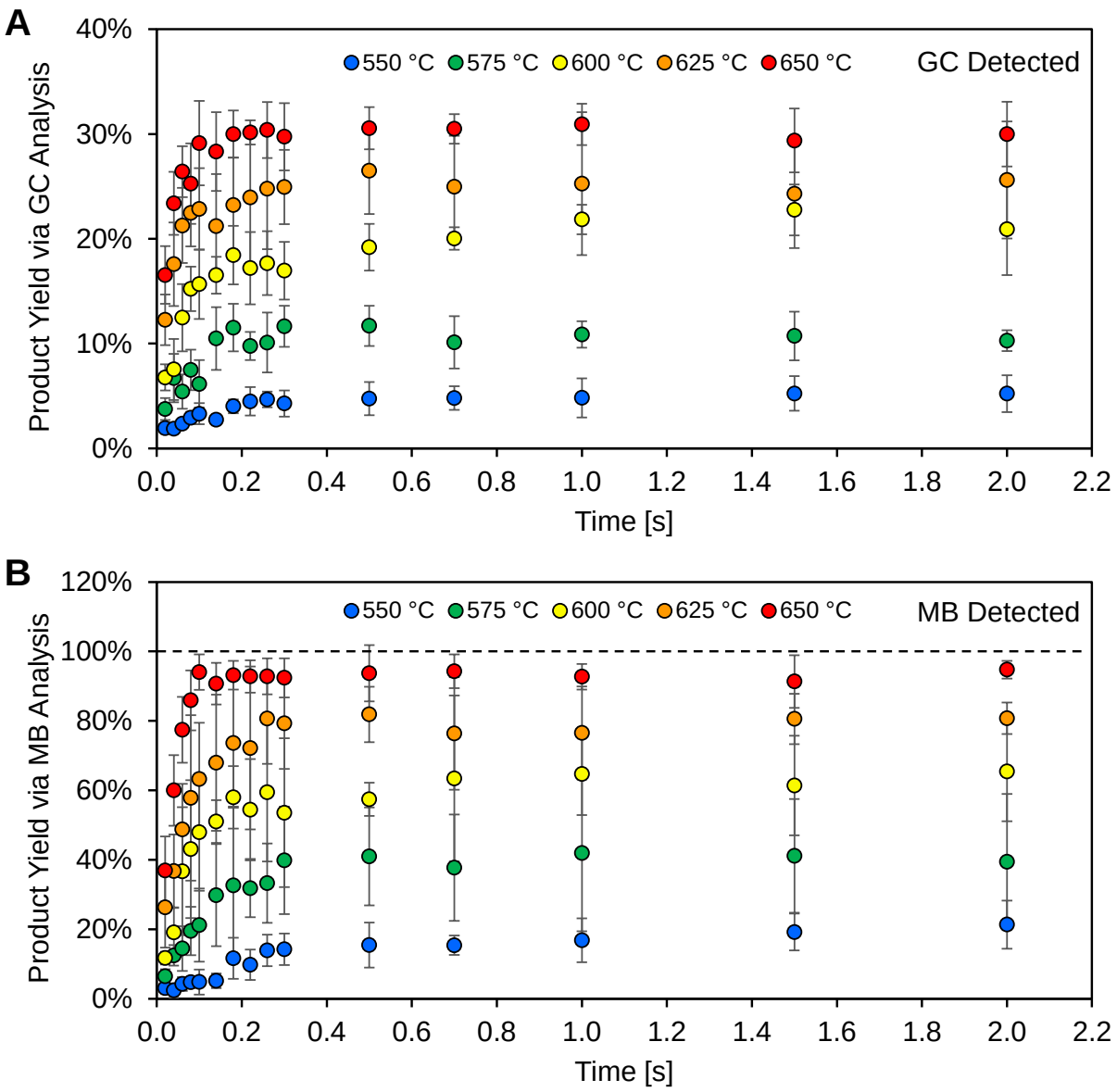

Figure 7. Yields of reacting low-density polyethylene thin films. (A) Yields detected by gas chromatography (GC). (B) Yields detected by microgram-resolution balance (MB).

remains over 100 °C cooler than the desired target temperature of 500 °C. Finally, **Figure 5c** summarizes the effects of sample thickness by comparing simulated temperature profiles through film samples from 15 to 500 µm in thickness. From this data, samples with thicknesses up to 25 µm demonstrate negligible heat transport limitations and maintain a uniform vertical temperature profile at the target temperature of the sample plate.

Because the results discussed thus far are order of magnitude estimates that rely on literature values, it was necessary to verify the predictions via experimental testing with the PHASR system. LDPE films were prepared with thicknesses from 8 to 100 µm, and at least three reactions for each thickness were conducted in the PHASR reactor for 100 ms at 650 °C. For each LDPE film sample, the product yield was measured by two methods (GC and microbalance) and plotted in **Figure 6**. The thinnest LDPE samples, 8 and 15 µm thick, produced the same yield of volatile products for both GC- and microbalance-detected species, indicating that heat and mass transport limitations are indeed absent at these sample thicknesses. In

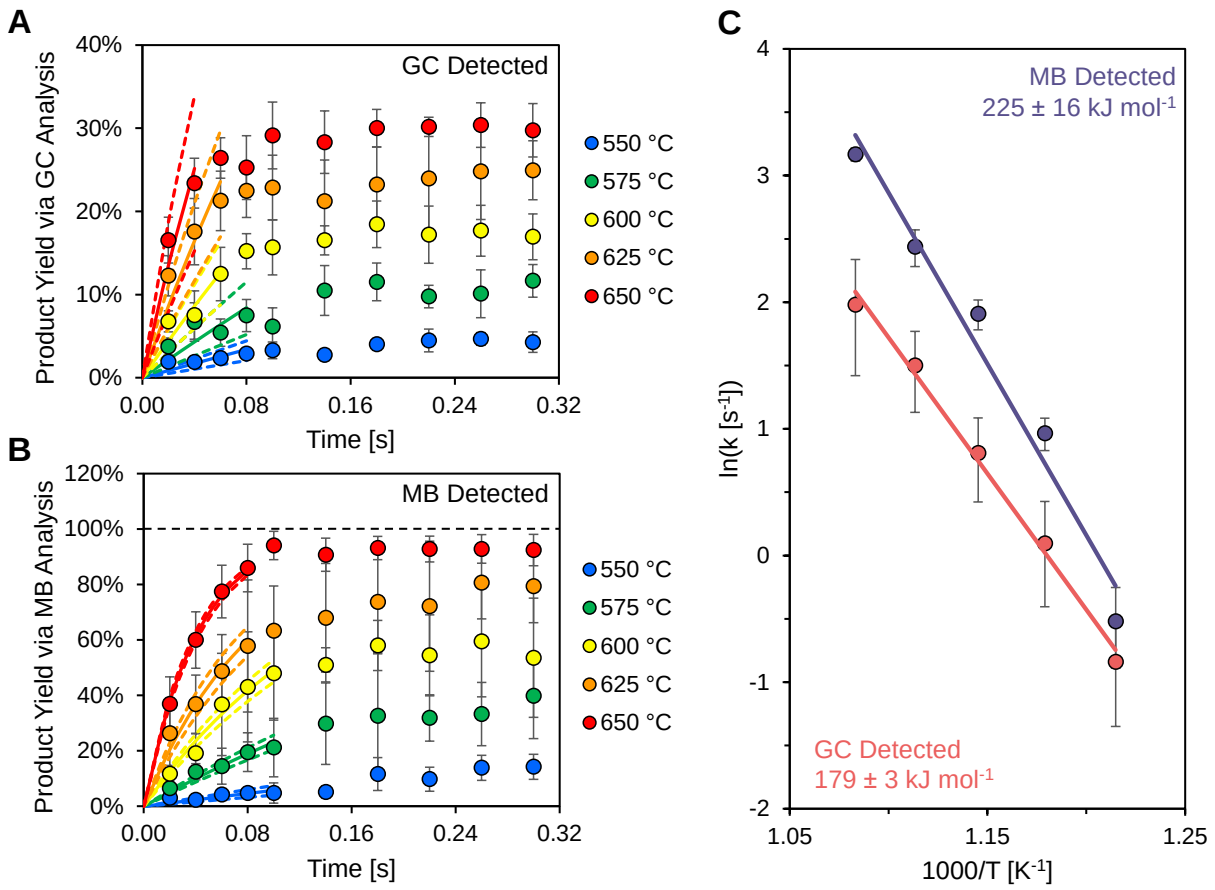

Figure 8. Yields and kinetic calculations of reacting low-density polyethylene thin films. (A) Short-time yields (measured experimentally: points; fit to first order model: lines) detected by gas chromatography (GC). (B) Short-time yields (measured experimentally: points; fit to first order model: lines) detected by microgram-resolution balance (MB). (C) Arrhenius plot for GC detected species (red) and MB detected species (purple), with linear regression for derivation of Arrhenius parameters. See Supporting Information for complete model fitting details.

contrast, for the 25, 50, and 100 µm thick samples, the yield of detectable products monotonically decreased, with thicker samples exhibiting progressively lower yields as a result of increasing transport limitations. From the dimensional analyses, heat transfer simulations, and varying film thickness experiments in PHASR, it can be concluded that the method of LDPE pyrolysis via PHASR enables operation under isothermal, reaction-controlled conditions, and the results obtained from this experimental method are intrinsic reaction kinetics.

3.2 Intrinsic Kinetics of LDPE Pyrolysis. Having verified the PHASR method is capable of pyrolyzing LDPE under isothermal, reaction-controlled conditions, a series of experiments was performed to measure the intrinsic reaction kinetic parameters. LDPE pyrolysis reactions were performed for reaction conditions spanning 550-650 °C and 20-2000 ms. The complete data set for these experiments is presented in **Figure 7**. GC-detected results are shown in **Figure 7a** and correspond to all detectable volatile products up to C20, while microbalance-detected results are shown in **Figure 7b** and correspond to yields based on the amount of remaining mass post-reaction. In both cases and for all evaluated temperatures, the observed yield achieves a maximum between about 180 ms (at 650 °C) and 500 ms (at 550 °C). Further increase of the GC- and microbalance-detected products is not detected within experimental error of the measurement at longer reaction times up to 2.0 s. This is consistent with the formation of residue on the passivated steel plate after reaction at all combinations of time and temperature, other

than at 650 °C after 180 ms of reaction; at 650 °C, the steel plates have no visible residue left behind, but a small amount is observed to be removed during the TCB cleaning process.

Using the yield data of **Figures 7a** and **7b**, several kinetic fitting models were evaluated via minimization of model/data error (i.e., best fit). Complete details for the kinetic fitting process are provided in the Supporting Information, but a first order consumption model, shown in **Equation 1**, was selected for the final fitting, since it both fit the data and is consistent with the reaction mechanisms of primary LDPE pyrolysis.

$$Y(t) = 1 - e^{-kt} \quad (1)$$

In **Figures 8a** and **8b**, the yield data shown in **Figure 7** has been truncated to focus on the initial region of short reaction time data that was used for kinetic parameter fitting, in which increasing reactivity was observed. In these plots, the model is plotted as a solid line for each temperature, and errors for the model are plotted as dashed lines. After fitting, an Arrhenius plot was generated for both the GC- and microbalance-detected data sets, as shown in **Figure 8c**. From the GC analysis, an activation energy (E_a) of 178.6 ± 2.5 kJ mol^{-1} and pre-exponential factor (reported in log form, $\ln(A)$) of 25.3 ± 0.6 ln(s^{-1}) were calculated, and from the microbalance analysis, the calculated values were 224.9 ± 15.7 kJ mol^{-1} and 32.6 ± 2.0 ln(s^{-1}), respectively. Additional detail about the Arrhenius parameter fitting is provided in the Supporting Information.

It is important to note that the microbalance analysis is more applicable to the overall intrinsic initial reaction kinetics of LDPE pyrolysis, as the microbalance-detected species encompass all products capable of volatilizing at a given reaction temperature. The GC analysis, as mentioned previously, captures product species up to C20 relevant for understanding the intrinsic initial reaction kinetics of light species production.

3.3 Comparison of Results to Literature Data. As shown in **Figure 2** and discussed previously, significant variation exists in the literature for the kinetic parameters of polyethylene pyrolysis. Apparent kinetics have been reported with results unique to the particular system under study. **Figure 2c** combines information from **Figures 2a** (literature-reported activation energy) and **2b** (literature-reported pre-exponential factor) into one graph, known as a 'compensation plot,' with additional information on reactor type (data point outline color), maximum reaction temperature (data point fill color), and sample size (data point size). 'Reactor type' was broadly divided into three categories: computational work and kinetic modeling, thermogravimetric analysis (TGA), and "custom," which accounts for all other experimental, non-TGA setups. Note that data point size is plotted on a log scale, though the smallest data points were reserved for studies that did not report sample size directly as mass. The kinetic data has also been converted to activation entropy (ΔS, corresponding to the right-side axis of **Figure 2c**) to enable calculation of a best fit (black line) for the compensation slope, which was determined to be 801 ± 33 K. Extensive detail about the literature used in this analysis is tabulated in the Supporting Information.

In this work, the intrinsic kinetics that have been measured are inherent to low-density polyethylene. The overall initial intrinsic kinetics described here, namely E_a = 224.9 ± 15.7 kJ mol^{-1} and $\ln(A)$ = 32.6 ± 2.0 ln(s^{-1}), exist well within the range of apparent values reported elsewhere in the literature (**Figure 2**). Similarly, the light species initial intrinsic kinetics, namely E_a = 178.6 ± 2.5 kJ mol^{-1} and $\ln(A)$ = 25.3 ± 0.6 ln(s^{-1}), are also consistent with the range of reported values. The kinetic parameters measured with PHASR for both sets of products (GC- and microbalance-detected) are toward the center of the distributions reported in **Figure 2**.

Furthermore, a Rice-Herzfeld radical reaction model was derived and applied to a generalized polyethylene pyrolysis system. The Rice-Herzfeld model is commonly used to describe radical reaction systems and simply defines generalized radical initiation, propagation, and termination steps.[14,33] After deriving associated rate equations and applying common simplifications, **Equation 2** was obtained as a final rate expression to describe polyethylene pyrolysis.

$$r_A = \frac{d[A]}{dt} = k_{2p}\left(\frac{2k_i}{k_t}\right)^{\frac{1}{2}}\left(\frac{[A]^{\frac{3}{2}}}{1+\frac{k_{2p}}{k_{3p}}[A]}\right) \quad (2)$$

In this equation, rate constants can be seen for initiation (k_i), propagation (k_{2p} and k_{3p}), and termination (k_t) steps, with species A identifying the original LDPE polymer. **Equation 2** can be further simplified to estimate apparent activation energies using DFT-calculated values for individual steps. In particular, DFT simulations were used to estimate activation energies for elementary alkane C-C bond cleavage (for k_i; ~360 kJ mol^{-1}), hydrogen abstraction from alkanes (for k_{2p}; ~48 kJ mol^{-1}), and alkane radical β-scission (for k_{3p}; ~120 kJ mol^{-1}). Termination reactions joining two radical species were assumed to have negligible energetic penalty (i.e., k_t was assumed to have an activation energy of 0 kJ mol^{-1}); however, different termination reactions (i.e., $\beta\beta$, $\beta\mu$, and $\mu\mu$) correspond to different reaction mechanisms. The calculation of overall apparent activation energy therefore changes based on which termination mechanism is assumed dominant, and using this approach, apparent activation energies of 228, 264, and 300 kJ mol^{-1} were estimated for $\beta\beta$-, $\beta\mu$-, and $\mu\mu$-dominant termination mechanisms, respectively. All of these values, estimated from first principles calculations, are consistent with the range of literature-reported values (**Figure 2**) and with the experimentally-determined values from the PHASR system. Full details regarding the Rice-Herzfeld model, derivation of **Equation 2**, application of DFT-calculated values, and comparison with PHASR data are provided in the Supporting Information.

Finally, the formation of unreactive residues at the temperatures in this study also has precedent in the literature. A number of studies report residue and char formation to varying degrees.[18,34–44] Heat and mass transfer limitations in other studies convolute product distributions due to extensive capability for secondary reactions (i.e., additional reactions of volatile components within the melt phase). Long residence times and non-uniformity in reporting product fractionation (i.e., identifying different product classes, such as "wax," "tar," and "residue," is not standardized) also complicates comparison with the literature. Significant unsaturation and aromaticity has been reported in residues and chars formed across a wide range of temperatures (300-800 °C),[18,34–44] typically attributed to short chain olefins enabling some combination of: 1) hydrogen abstraction and acetylene addition, and 2) dehydrogenation and Diels-Alder condensation.[18,36,39] Additionally, the extent of residue formation appears to be a nonlinear function of temperature. At lower temperatures (<420 °C), residue has been shown to account for over 80% of total yield, even after reaction durations over one hour.[34] At intermediate temperatures (~425 to ~500 °C), significant amounts of alkenes and aromatics are still present, accounting for up to ~20% of total yield.[39,44] From ~500 to ~650 °C, residue formation reaches a minimum,[37,42] and then aromatics content begins increasing again as temperatures increase up to ~800 °C and beyond.[35,40,42] Again, it is important to note that the product fractionation reported elsewhere is not necessarily directly comparable with the results from PHASR, but the trends highlighted above are generally consistent with the plateauing yields and residue formation observed in these studies with PHASR.

3.4 Analysis of Pyrolysis Residues. Due to the existence of residue after pyrolysis at all reaction conditions other than at 650 °C beyond 100 ms, efforts were made to characterize this residue. The primary challenge in this regard is the small amount of sample required to maintain isothermal, reaction-controlled operation in PHASR. With PHASR LDPE samples initially being 80 ± 10 µg, residues left after reaction are of order 10 µg. These residues are attached to the passivated sample plate and behave like char. During initial testing for possible cleaning procedures, scraping the residue with tweezers or other instruments proved unsuccessful, and the only solvent able to completely remove it within a reasonable timeframe was heated 1,2,4-trichlorobenzene (TCB). Photographs taken through an optical microscope are shown in **Figure 9** and illustrate the different appearance of the residues after reaction durations of 20 and 2000 ms at 550 °C. The LDPE sample reacted for 20 ms at 550 °C (**Figure 9a**) has evidence of bubbling caused by gas and vapor species volatilizing off the passivated steel plate, and the sample retains its original ~3.0 mm diameter round shape, similar to an unreacted LDPE film. In contrast, the LDPE sample reacted for 2000 ms at 550 °C (**Figure 9b**) has deformed significantly, and parts of it are dark and demonstrate a char-like appearance. Sample movement is an indication of a possible Leidenfrost effect, something that was reported with LDPE at

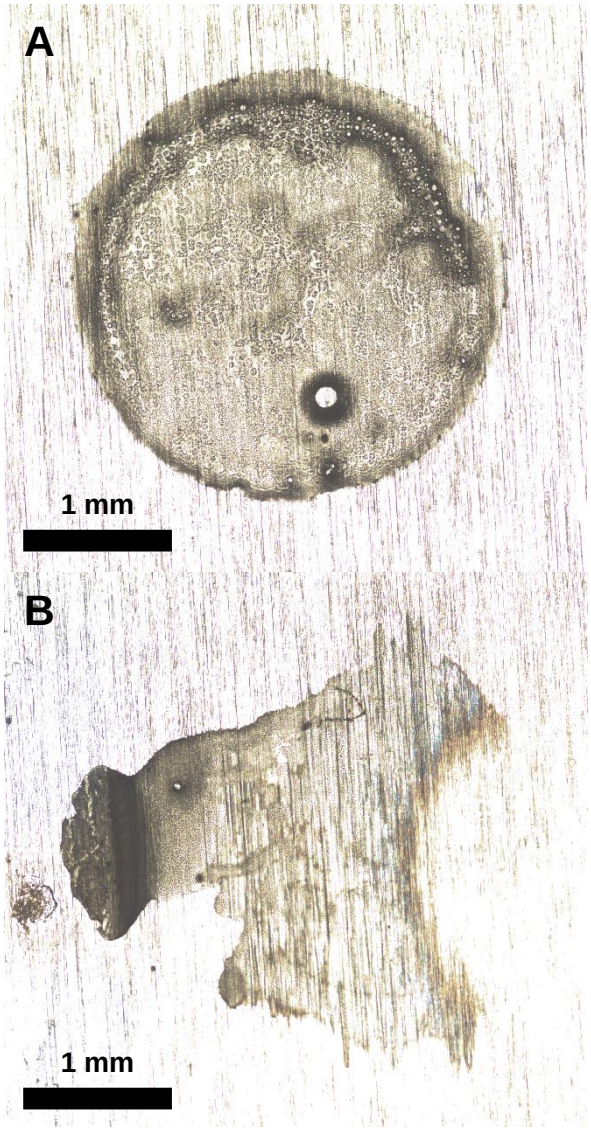

Figure 9. Images taken with a 5x lens after reaction in PHASR using an optical microscope. (A) Low-density polyethylene sample after 20 ms of reaction time at 550 °C. (B) Low-density polyethylene sample after 2.0 s of reaction time at 550 °C.

intermediate temperatures (particularly in the ~550-600 °C range) for the first time in a previous work.[8]

Because samples are small and the cleaning process requires soaking in non-negligible amounts of TCB, dissolved residues were very dilute (~1 µg mL^{-1}) and unable to be characterized via traditional means like liquid chromatography (LC) or gel permeation chromatography (GPC), which require concentrations of ~1 mg mL^{-1} to be effective. Preliminary testing was conducted with thicker LDPE films (250 µm thick) to enable ^{13}C solid state NMR analysis, but the previously-discussed

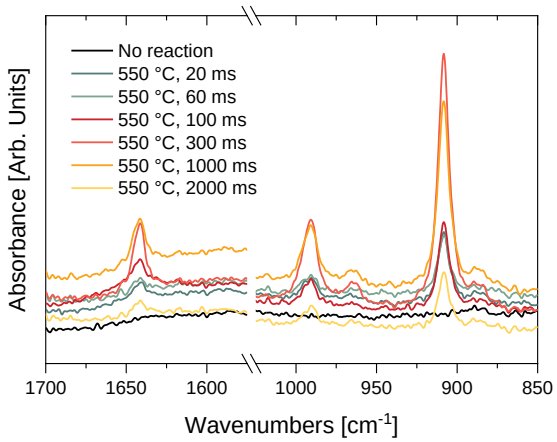

Figure 10. Advanced attenuated total reflectance infrared (ATR-IR) corrected spectroscopy of low-density polyethylene samples after reaction at 550 °C for varying durations (20 ms to 2000 ms, various colors), along with an unreacted sample (black) for comparison. All reacted samples were analyzed after quenching to room temperature within the PHASR reactor.

transport limitations arising at this thickness ensured that most of the film remained unreacted, and the resulting NMR spectrum was comparable to that of unreacted LDPE. Thermogravimetric analysis (TGA) was also conducted with the residues, but it proved similarly unsuccessful, primarily due to: 1) inaccurate weight measurement during heating ramps (the mass of residue was order 10 µg, versus a steel plate mass of order 10 mg), and 2) residual oxygen on the steel surface facilitating residue burn off. Additionally, Raman spectroscopy was conducted on residues after 550 °C reaction for durations between 20 and 2000 ms, as well as on an unreacted LDPE film and a bare steel plate. In all cases other than the bare plate, the same spectrum of peaks was observed. Further detail on the NMR, TGA, and Raman studies is provided in the Supporting Information.

ATR-IR spectroscopy and Advanced ATR-IR Corrected spectroscopy were conducted on the same set of samples used for Raman spectroscopy, with additional detail available in the Supporting Information. **Figure 10** highlights the key infrared spectroscopy results. For all reacted samples, new peaks emerged at 1641, 991, and 908 cm^{-1} that did not exist in the original, unreacted LDPE sample. These peaks correspond to aromatic and multi-substituted alkene species.[45,46] The IR spectra are consistent with the formation of unsaturated

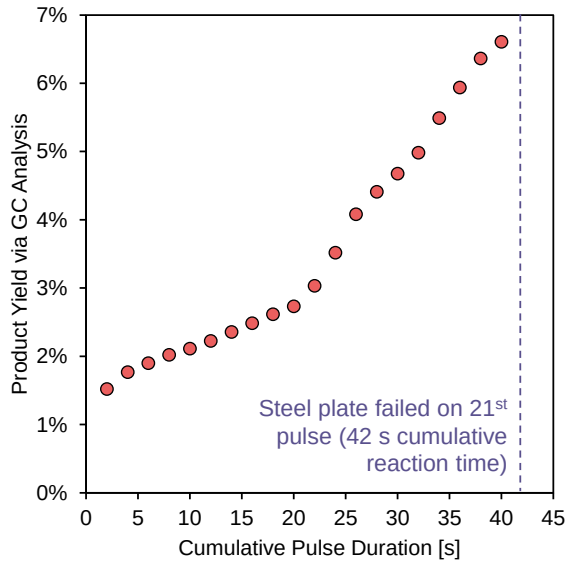

Figure 11. Cumulative yield of a low-density polyethylene film over the course of 20 successive reaction pulses, each of temperature 500 °C and duration 2.0 s, for a cumulative reaction duration of 40 s. The passivated steel plate failed on the 21st reaction pulse.

precursors to polyaromatic char product that yields a maximum in conversion to volatile products, as observed in **Figures 7a** and **7b** in the first two seconds of reaction.

3.5 Secondary LDPE Pyrolysis Kinetics. The solid residue formed in the first two seconds of reaction by PHASR, which has a lower degree of saturation as shown by spectroscopy, could be an endpoint of the reaction, or it could continue to react with new chemistry at a slower timescale not detectable in the temporal range of the PHASR reactor. The PHASR experimental power controller is designed for powerful, millisecond pulses of electrical current, and an inbuilt safety function that cannot be circumvented prohibits pulses longer than 2.0 s, as described elsewhere.[8] Therefore, reaction durations longer than 2.0 s at 550-650 °C with a single PHASR pulse cannot be conducted with the current millisecond controller setup.

To probe the stability of the solid residue, an exploratory experiment was conducted that consisted of successive PHASR pulses to solid LDPE pyrolysis residue. The challenge of this experimental sequence exists with the PHASR sample plate; the passivated steel plates, which are only 0.007" thick, experience extreme electrical and thermal stresses during repeated electrical pulsing (i.e., heating to >550 °C in <20 ms via a ~1.3 kA current, maintaining temperature for 2.0 s, cooling to room temperature in <180 ms). Of the dozens of samples that have undergone multiple pulse testing, only one PHASR plate with LDPE sample residue has remained intact for greater than four 2.0 s pulses (8.0 s cumulative reaction time), even at reduced temperature (500 °C) to require slightly less current being applied (~1.2 kA instead of ~1.3 kA). The results of this experiment are shown in **Figure 11**, which demonstrates the cumulative yield of GC-detected species up to 40 s via 20 successive reaction pulses at 500 °C (2.0 s per pulse). Consistent with the reactions at 550-650 °C, the first two seconds of PHASR pulse at 500 °C (**Figure 11**, leftmost data point) produced only a small amount of GC-detectable products (~1.5%). However, the successive 19 PHASR pulses at 500 °C for 2.0 s indicated that the solid residue continued to react with monotonically increasing cumulative yield of GC-detectable products, with a

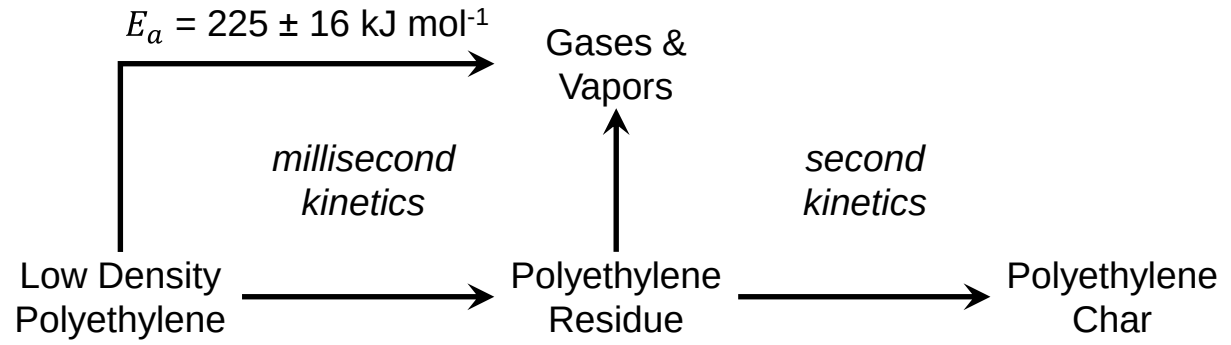

Scheme 1. Pyrolysis of low-density polyethylene exhibits millisecond kinetics at 550-650 °C to form gases, vapors, and polyethylene residue, after which slower decomposition kinetics produce gases, vapors, and char on the timescale of seconds.

final observed cumulative yield of ~6.5% before plate failure.

The continued reactivity of solid residue produced in the PHASR reactor after 2.0 s indicates the existence of a second set of pyrolysis reactions that are much slower than the millisecond reactions that occur in the first ~0.5 s of LDPE pyrolysis. As observed in **Figure 7**, yields for both GC- and microbalance-detected species plateaued at a maximum yield for all evaluated temperatures during one reaction pulse of duration 2.0 s. During this initial two seconds, the spectroscopic results of **Figure 10** indicate that the original solid LDPE increases in degree of unsaturation, concomitant with the formation of a dark, char-like color visible in microscope photographs (**Figure 9**). The secondary solid-phase reactions are thus likely significantly slower due to the chemical nature of the pyrolysis residue. As depicted in **Scheme 1**, LDPE pyrolysis at temperatures of 550-650 °C can be depicted as a two-part lumped reaction system; millisecond kinetics initially yield gases and vapors with an accompanying pyrolysis residue, which further reacts on the timescale of seconds to form additional vapors and gases with a solid, unreactive char. Future work will utilize a new PHASR controller system that permits quantitative kinetic measurements of the slower, second-timescale kinetics of LDPE pyrolysis.

4.0 Conclusions. Pyrolysis of low-density polyethylene (LDPE) has been evaluated in the temperature range of 550-650 °C for reaction durations of 20 ms up to 2.0 s using the method of Pulse-Heated Analysis of Solid Reactions (PHASR). The PHASR system reacts LDPE film samples ~15 μm thick in the absence of heat and mass transfer limitations, as confirmed by experiments with LDPE samples of varying thickness. The intrinsic kinetics of LDPE pyrolysis were measured via two reaction metrics: 1) the quantity of detectable products quantified in a gas chromatograph up to C20, and 2) the quantity of material that volatilized from the sample plate as detected by post-reaction measurements with a microgram-resolution balance. Both methods indicate incomplete conversion of LDPE to volatile products at temperatures of 550-625 °C for reaction durations of up to 2.0 s; only pyrolysis of LDPE at 650 °C achieved complete volatilization, which occurred after ~100 ms. When fit to a first order lumped reaction model with rate coefficient, k, the millisecond kinetics of volatile product formation based on microbalance-detected products exhibited an intrinsic activation energy of 225 ± 16 kJ mol^{-1}. The resulting solid residue after two seconds of reaction exhibited a darker color than the original LDPE sample, and infrared spectroscopy indicated an increase in the degree of unsaturated bonds. The slower, secondary chemistry of LDPE pyrolysis residue, occurring over seconds of time, will be the focus of future work.

Acknowledgements. We acknowledge financial support from the ExxonMobil Technology and Engineering Company, and from the University of Minnesota Center for Sustainable Polymers, under grant number CHE-1901635. Parts of this work were carried out in the University of Minnesota Characterization Facility, which receives partial support from NSF through the MRSEC program. The Raman and ATR-IR spectroscopy used for residue characterization were conducted by and analyzed in consultation with Characterization Facility technician Bing Luo.

Keywords. flash pyrolysis, kinetics, polyethylene, pyrolysis, recycling

Supporting Information. The Supporting Information is available online.

References.

(1) Geyer, R.; Jambeck, J. R.; Law, K. L. Production, Use, and Fate of All Plastics Ever Made. *Sci. Adv.* **2017**, *3* (7), e1700782. https://doi.org/10.1126/sciadv.1700782.

(2) Borrelle, S. B.; Ringma, J.; Law, K. L.; Monnahan, C. C.; Lebreton, L.; McGivern, A.; Murphy, E.; Jambeck, J.; Leonard, G. H.; Hilleary, M. A.; Eriksen, M.; Possingham, H. P.; De Frond, H.; Gerber, L. R.; Polidoro, B.; Tahir, A.; Bernard, M.; Mallos, N.; Barnes, M.; Rochman, C. M. Predicted Growth in Plastic Waste Exceeds Efforts to Mitigate Plastic Pollution. *Science (80-.).* **2020**, *369* (6510), 1515–1518. https://doi.org/10.1126/science.aba3656.

(3) *Global Waste Management Outlook*; United Nations, 2016. https://doi.org/10.18356/765baec0-en.

(4) Lau, W. W. Y.; Shiran, Y.; Bailey, R. M.; Cook, E.; Stuchtey, M. R.; Koskella, J.; Velis, C. A.;

Godfrey, L.; Boucher, J.; Murphy, M. B.; Thompson, R. C.; Jankowska, E.; Castillo Castillo, A.; Pilditch, T. D.; Dixon, B.; Koerselman, L.; Kosior, E.; Favoino, E.; Gutberlet, J.; Baulch, S.; Atreya, M. E.; Fischer, D.; He, K. K.; Petit, M. M.; Sumaila, U. R.; Neil, E.; Bernhofen, M. V.; Lawrence, K.; Palardy, J. E. Evaluating Scenarios toward Zero Plastic Pollution. *Science (80-.).* **2020**, *369* (6510), 1455–1461. https://doi.org/10.1126/science.aba9475.

(5) Mathews, J. A.; Tan, H. Circular Economy: Lessons from China. *Nature* **2016**, *531* (7595), 440–442. https://doi.org/10.1038/531440a.

(6) Somoza-Tornos, A.; Gonzalez-Garay, A.; Pozo, C.; Graells, M.; Espuna, A.; Guillén-Gosálbez, G. Realizing the Potential High Benefits of the Circular Economy in the Chemical Industry: Ethylene Monomer Recovery via Polyethylene Pyrolysis. *ACS Sustain. Chem. Eng.* **2020**, acssuschemeng.9b04835. https://doi.org/10.1021/acssuschemeng.9b04835.

(7) Rabnawaz, M.; Wyman, I.; Auras, R.; Cheng, S. A Roadmap towards Green Packaging: The Current Status and Future Outlook for Polyesters in the Packaging Industry. *Green Chem.* **2017**, *19* (20), 4737–4753. https://doi.org/10.1039/C7GC02521A.

(8) Zolghadr, A.; Sidhu, N.; Mastalski, I.; Facas, G.; Maduskar, S.; Uppili, S.; Go, T.; Neurock, M.; Dauenhauer, P. J. On the Method of Pulse-Heated Analysis of Solid Reactions (PHASR) for Polyolefin Pyrolysis. *ChemSusChem* **2020**, cssc.202002667. https://doi.org/10.1002/cssc.202002667.

(9) Mark, L. O.; Cendejas, M. C.; Hermans, I. The Use of Heterogeneous Catalysis in the Chemical Valorization of Plastic Waste. *ChemSusChem* **2020**, *13* (22), 5808–5836. https://doi.org/10.1002/cssc.202001905.

(10) Coates, G. W.; Getzler, Y. D. Y. L. Chemical Recycling to Monomer for an Ideal, Circular Polymer Economy. *Nat. Rev. Mater.* **2020**, *5* (7), 501–516. https://doi.org/10.1038/s41578-020-0190-4.

(11) Qureshi, M. S.; Oasmaa, A.; Pihkola, H.; Deviatkin, I.; Tenhunen, A.; Mannila, J.; Minkkinen, H.; Pohjakallio, M.; Laine-Ylijoki, J. Pyrolysis of Plastic Waste: Opportunities and Challenges. *J. Anal. Appl. Pyrolysis* **2020**, *152* (February), 104804. https://doi.org/10.1016/j.jaap.2020.104804.

(12) Hahladakis, J. N.; Velis, C. A.; Weber, R.; Iacovidou, E.; Purnell, P. An Overview of Chemical Additives Present in Plastics: Migration, Release, Fate and Environmental Impact during Their Use, Disposal and Recycling. *J. Hazard. Mater.* **2018**, *344*, 179–199. https://doi.org/10.1016/j.jhazmat.2017.10.014.

(13) Kaminsky, W.; Schiers, J. *Feedstock Recycling and Pyrolysis of Waste Plastics*; Scheirs, J., Kaminsky, W., Eds.; John Wiley & Sons, Ltd: Chichester, UK, 2006; Vol. 2006. https://doi.org/10.1002/0470021543.

(14) Rice, F. O. The Thermal Decomposition Of Organic Compounds From The Standpoint Of Free Radicals. I. Saturated Hydrocarbons. *J. Am. Chem. Soc.* **1931**, *53* (5), 1959–1972. https://doi.org/10.1021/ja01356a053.

(15) Rice, F. O.; Glasebrook, A. L. The Thermal Decomposition of Organic Compounds from the Standpoint of Free Radicals. VII. The Ethylidene Radical. *J. Am. Chem. Soc.* **1934**, *56* (3), 741–743. https://doi.org/10.1021/ja01318a066.

(16) Bockhorn, H.; Hornung, A.; Hornung, U. Mechanisms and Kinetics of Thermal Decomposition of Plastics from Isothermal and Dynamic Measurements. *J. Anal. Appl. Pyrolysis* **1999**, *50* (2), 77–101. https://doi.org/10.1016/S0165-2370(99)00026-1.

(17) Bockhorn, H.; Hornung, A.; Hornung, U.; Schawaller, D. Kinetic Study on the Thermal Degradation of Polypropylene and Polyethylene. *J. Anal. Appl. Pyrolysis* **1999**, *48* (2), 93–109. https://doi.org/10.1016/S0165-2370(98)00131-4.

(18) Williams, P. T.; Williams, E. A. Fluidised Bed Pyrolysis of Low Density Polyethylene to Produce Petrochemical Feedstock. *J. Anal. Appl. Pyrolysis* **1999**, *51* (1–2), 107–126. https://doi.org/10.1016/S0165-2370(99)00011-X.

(19) Poutsma, M. L. Fundamental Reactions of Free Radicals Relevant to Pyrolysis Reactions. *J. Anal. Appl. Pyrolysis* **2000**, *54* (1–2), 5–35. https://doi.org/10.1016/S0165-2370(99)00083-2.

(20) Levine, S. E.; Broadbelt, L. J. Detailed Mechanistic Modeling of High-Density Polyethylene Pyrolysis: Low Molecular Weight Product Evolution. *Polym. Degrad. Stab.* **2009**, *94* (5), 810–822. https://doi.org/10.1016/j.polymdegradstab.2009.01.031.

(21) Popov, K. V.; Knyazev, V. D. Initial Stages of the Pyrolysis of Polyethylene. *J. Phys. Chem. A* **2015**, *119* (49), 11737–11760. https://doi.org/10.1021/acs.jpca.5b07440.

(22) Kiran, E.; Gillham, J. K. Pyrolysis-Molecular Weight Chromatography: A New on-Line System for Analysis of Polymers. II. Thermal Decomposition of Polyolefins: Polyethylene, Polypropylene, Polyisobutylene. *J. Appl. Polym. Sci.* **1976**, *20* (8), 2045–2068. https://doi.org/10.1002/app.1976.070200803.

(23) Ceamanos, J.; Mastral, J. .; Millera, A.; Aldea, M. . Kinetics of Pyrolysis of High Density Polyethylene. Comparison of Isothermal and Dynamic Experiments. *J. Anal. Appl. Pyrolysis* **2002**, *65* (2), 93–110. https://doi.org/10.1016/S0165-2370(01)00183-8.

(24) Ranzi, E.; Dente, M.; Goldaniga, A.; Bozzano, G.; Faravelli, T. Lumping Procedures in Detailed Kinetic Modeling of Gasification, Pyrolysis, Partial Oxidation and Combustion of Hydrocarbon Mixtures. *Prog. Energy Combust. Sci.* **2001**, *27* (1), 99–139. https://doi.org/10.1016/S0360-1285(00)00013-7.

(25) Dogu, O.; Pelucchi, M.; Van de Vijver, R.; Van Steenberge, P. H. M.; D'hooge, D. R.; Cuoci, A.; Mehl, M.; Frassoldati, A.; Faravelli, T.; Van Geem, K. M. The Chemistry of Chemical Recycling of Solid Plastic Waste via Pyrolysis and Gasification: State-of-the-Art, Challenges, and Future Directions. *Prog. Energy Combust. Sci.* **2021**, *84* (2), 100901. https://doi.org/10.1016/j.pecs.2020.100901.

(26) Harmon, R. E.; SriBala, G.; Broadbelt, L. J.; Burnham, A. K. Insight into Polyethylene and Polypropylene Pyrolysis: Global and Mechanistic Models. *Energy & Fuels* **2021**, *35* (8), 6765–6775. https://doi.org/10.1021/acs.energyfuels.1c00342.

(27) Faravelli, T.; Bozzano, G.; Scassa, C.; Perego, M.; Fabini, S.; Ranzi, E.; Dente, M. Gas Product Distribution from Polyethylene Pyrolysis. *J. Anal. Appl. Pyrolysis* **1999**, *52* (1), 87–103. https://doi.org/10.1016/S0165-2370(99)00032-7.

(28) Al-Salem, S. M.; Lettieri, P. Kinetic Study of High Density Polyethylene (HDPE) Pyrolysis. *Chem. Eng. Res. Des.* **2010**, *88* (12), 1599–1606. https://doi.org/10.1016/j.cherd.2010.03.012.

(29) Williams, E. A.; Williams, P. T. Analysis of Products Derived from the Fast Pyrolysis of Plastic Waste. *J. Anal. Appl. Pyrolysis* **1997**, *40–41*, 347–363. https://doi.org/10.1016/S0165-2370(97)00048-X.

(30) Sezgi, N. A.; Cha, W. S.; Smith, J. M.; McCoy, B. J. Polyethylene Pyrolysis: Theory and Experiments for Molecular-Weight-Distribution Kinetics. *Ind. Eng. Chem. Res.* **1998**, *37* (7), 2582–2591. https://doi.org/10.1021/ie980106r.

(31) Teixeira, A. R.; Gantt, R.; Joseph, K. E.; Maduskar, S.; Paulsen, A. D.; Krumm, C.; Zhu, C.; Dauenhauer, P. J. Spontaneous Aerosol Ejection: Origin of Inorganic Particles in Biomass Pyrolysis. *ChemSusChem* **2016**, *9* (11), 1322–1328. https://doi.org/10.1002/cssc.201600112.

(32) Krumm, C.; Pfaendtner, J.; Dauenhauer, P. J. Millisecond Pulsed Films Unify the Mechanisms of Cellulose Fragmentation. *Chem. Mater.* **2016**, *28* (9), 3108–3114. https://doi.org/10.1021/acs.chemmater.6b00580.

(33) Rice, F. O.; Johnston, W. R.; Evering, B. L. THE THERMAL DECOMPOSITION OF ORGANIC COMPOUNDS FROM THE STANDPOINT OF FREE RADICALS. II. EXPERIMENTAL EVIDENCE OF THE DECOMPOSITION OF ORGANIC COMPOUNDS INTO FREE RADICALS. *J. Am. Chem. Soc.* **1932**, *54* (9), 3529–3543. https://doi.org/10.1021/ja01348a007.

(34) Madorsky, S. L.; Straus, S.; Thompson, D.; Williamson, L. Pyrolysis of Polyisobutene (Vistanex), Polyisoprene, Polybutadiene, GR-S, and Polyethylene in a High Vacuum. *J. Res. Natl. Bur. Stand. (1934).* **1949**, *42* (5), 499. https://doi.org/10.6028/jres.042.044.

(35) Jung, S.-H.; Cho, M.-H.; Kang, B.-S.; Kim, J.-S. Pyrolysis of a Fraction of Waste Polypropylene and Polyethylene for the Recovery of BTX Aromatics Using a Fluidized Bed Reactor. *Fuel Process. Technol.* **2010**, *91* (3), 277–284. https://doi.org/10.1016/j.fuproc.2009.10.009.

(36) Lopez, G.; Artetxe, M.; Amutio, M.; Alvarez, J.; Bilbao, J.; Olazar, M. Recent Advances in the Gasification of Waste Plastics. A Critical Overview. *Renew. Sustain. Energy Rev.* **2018**, *82* (September 2017), 576–596. https://doi.org/10.1016/j.rser.2017.09.032.

(37) Koo, J.-K.; Kim, S.-W.; Seo, Y.-H. Characterization of Aromatic Hydrocarbon Formation from Pyrolysis of Polyethylene-Polystyrene Mixtures. *Resour. Conserv. Recycl.* **1991**, *5* (4), 365–382. https://doi.org/10.1016/0921-3449(91)90013-E.

(38) Conesa, J. A.; Font, R.; Marcilla, A.; Garcia, A. N. Pyrolysis of Polyethylene in a Fluidized Bed Reactor. *Energy & Fuels* **1994**, *8* (6), 1238–1246. https://doi.org/10.1021/ef00048a012.

(39) McCaffrey, W. C.; Kamal, M. R.; Cooper, D. G. Thermolysis of Polyethylene. *Polym. Degrad. Stab.* **1995**, *47* (1), 133–139. https://doi.org/10.1016/0141-3910(94)00096-Q.

(40) Cozzani, V.; Nicolella, C.; Rovatti, M.; Tognotti, L. Influence of Gas-Phase Reactions on the Product Yields Obtained in the Pyrolysis of Polyethylene. *Ind. Eng. Chem. Res.* **1997**, *36* (2), 342–348. https://doi.org/10.1021/ie950779z.

(41) Predel, M.; Kaminsky, W. Pyrolysis of Mixed Polyolefins in a Fluidized-Bed Reactor and on a Pyro-GC/MS to Yield Aliphatic Waxes. *Polym. Degrad. Stab.* **2000**, *70* (3), 373–385. https://doi.org/10.1016/S0141-3910(00)00131-2.

(42) Mastellone, M. L.; Perugini, F.; Ponte, M.; Arena, U. Fluidized Bed Pyrolysis of a Recycled Polyethylene. *Polym. Degrad. Stab.* **2002**, *76* (3), 479–487. https://doi.org/10.1016/S0141-

3910(02)00052-6.
(43) Hernández, M. del R.; Gómez, A.; García, Á. N.; Agulló, J.; Marcilla, A. Effect of the Temperature in the Nature and Extension of the Primary and Secondary Reactions in the Thermal and HZSM-5 Catalytic Pyrolysis of HDPE. *Appl. Catal. A Gen.* **2007**, *317* (2), 183–194. https://doi.org/10.1016/j.apcata.2006.10.017.
(44) Onwudili, J. A.; Insura, N.; Williams, P. T. Composition of Products from the Pyrolysis of Polyethylene and Polystyrene in a Closed Batch Reactor: Effects of Temperature and Residence Time. *J. Anal. Appl. Pyrolysis* **2009**, *86* (2), 293–303. https://doi.org/10.1016/j.jaap.2009.07.008.
(45) Beauchamp, P. Spectroscopy Tables http://www.cpp.edu/~psbeauchamp/pdf/spec_ir_nmr_spectra_tables.pdf.
(46) Shimanouchi, T. Tables of Molecular Vibrational Frequencies: Part 6. *J. Phys. Chem. Ref. Data* **1973**, *2* (1), 121–162. https://doi.org/10.1063/1.3253114.